RSC Advances

PAPER

View Article Online
View Journal | View Issue

Cite this: *RSC Adv.*, 2024, **14**, 23232

Nanocellulose reinforced polyvinyl alcohol-based bio-nanocomposite films: improved mechanical, UV-light barrier, and thermal properties

Melbi Mahardika, *[abc] Nanang Masruchin,[abc] Devita Amelia,[d] Rushdan Ahmad Ilyas,[bde] Athanasia Amanda Septevani,[bf] Edi Syafri,[bg] Novitri Hastuti,[ab] Myrtha Karina,[abc] Moonis Ali Khan,[h] Byong-Hun Jeon[i] and Nasmi Herlina Sari[j]

This study reported the development and characterisation of bio-nanocomposite films based on the polyvinyl alcohol (PVA) reinforced with cellulose nanofibres (CNFs) of different concentrations (1–5 wt%), isolated from pineapple leaf fibre *via* high-shear homogenisation and ultrasonication. The PVA film and bio-nanocomposite were prepared using a solution casting method. The PVA film and bio-nanocomposite samples were characterized using FE-SEM, XRD, FTIR spectroscopy, UV-vis spectroscopy in transmission mode, TGA, and DTG. Mechanical properties (tensile strength and strain at break) were also determined and statistical analysis was applied as well. With the incorporation of CNFs, the mechanical properties of the bio-nanocomposite were found to be significant ($p \leq 0.05$), particularly the 4 wt% CNF bio-nanocomposite showed optimum properties. The tensile strength, CI, and thermal stability of this film were 28.9 MPa (increased by 28.2%), 78.7% (increased by 5.2%), and 341.8 °C (increased by 1.6%), respectively, compared to the pure PVA film. These characteristics imply that the bio-nanocomposite film has prospects as a promising material for biopackaging.

Received 8th June 2024
Accepted 15th July 2024

DOI: 10.1039/d4ra04205k

rsc.li/rsc-advances

1. Introduction

Nowadays, the most dominating pollution in the world comes from plastic wastes, especially petroleum-based plastic wastes.[1] Packaging plastics are generally made from non-renewable petroleum products.[2–5] They are non-biodegradable and take a long time to decompose naturally in the environment.[6] The presence and accumulation of plastic waste in the environment are harmful to the ecosystem and humans.[7]

Polyvinyl alcohol (PVA)-based bioplastics are a promising alternative to replace conventional plastics in everyday life. PVA is a biodegradable polymer with many advantages, such as being non-toxic, low-cost, and easy to process.[8,9] In Indonesia, biocomposite plastic companies have been operating since 2009. They are developing biopolymers as bioplastic matrices. Among them, PT. Inter Aneka Lestari Kimia or better known as Enviplast is developing biopolymers and even exporting them to various countries globally. However, PVA-based biocomposites tend to have poor mechanical properties.[10,11] PVA films at certain temperatures and conditions can dissolve in water, so the use of PVA as a composite is very limited and needs modifications.[12] The properties of PVA are determined by the molecular weight and the degree of hydrolysis which is influenced by the length of the vinyl acetate used when producing PVA. The molecular weight of PVA generally ranges from 20 000–400 000 g mol^{-1}.[13] The addition of fillers or reinforcement to the PVA matrix using natural fibre can solve the limitation of the PVA application.

Natural fibres are eco-friendly materials that can be derived from plants, animals, and minerals, depending on the source of extraction.[14] Natural fibres have been used as reinforcement for biocomposites and are suitable for many industrial applications.[15,16] Special treatment is needed to isolate cellulose from the plant cell wall to obtain natural fibre from a plant.[17–19]

[a]*Research Center for Biomass and Bioproducts, National Research and Innovation Agency of Indonesia (BRIN), Cibinong, 16911, Indonesia. E-mail: melbi.mahardika@brin.go.id*

[b]*Research Collaboration Center for Nanocellulose, BRIN and Andalas University, Padang, 25163, Indonesia*

[c]*Research Collaboration Center for Biomass and Biorefinery between BRIN and Universitas Padjadjaran, Jatinangor, 45363, Indonesia*

[d]*Faculty of Chemical and Energy Engineering, Universiti Teknologi Malaysia, 81310 UTM Johor Bahru, Johor, Malaysia*

[e]*Centre for Advanced Composite Materials, Universiti Teknologi Malaysia, 81310 UTM Johor Bahru, Johor, Malaysia*

[f]*Research Center for Environmental and Clean Technology, National Research and Innovation Agency, Komplek BRIN Cisitu, Bandung, 40135, Indonesia*

[g]*Department of Agricultural Technology, Politeknik Pertanian Negeri Payakumbuh, West Sumatra, 26271, Indonesia*

[h]*Chemistry Department, College of Science, King Saud University, Riyadh, 11451, Saudi Arabia*

[i]*Department of Earth Resources and Environmental Engineering, Hanyang University, Seoul 04763, Republic of Korea*

[j]*Department of Mechanical Engineering, Faculty of Engineering, University of Mataram, Mataram 83125, Indonesia*

Natural fibres contain cellulose, hemicellulose, lignin, and extractive substances. The non-cellulose content of fibre can be removed by the chemical treatments such as alkalisation and bleaching.[20–23] The advantages of natural fibres include economic, abundant availability, low specific gravity, high specific resistance, high rigidity, renewable resources, biodegradability, lower energy consumption for production, lower CO_2 emissions, and being environmentally friendly.[24] Many sources of fibres have been used in biocomposites, including date palms,[25] elephant grass,[26] sugarcane stem,[27] cellulose from jicama,[28] and pineapple leaf.[29] Noshirvani *et al.* (2018) extracted cellulose nanocrystals from a cotton linter and used it as a bio-nanocomposite filler.[30] It improved the crystallinity, thermal stability, and mechanical properties of biocomposite. Choo *et al.* (2016) also found a similar result using cellulose nanofibres as fillers for biopolymer matrix.[31] The addition of bagasse nanofibrils increased the film's crystallinity, tensile stress, and thermal stability.[32]

Previous research has not investigated the impact of varied cellulose nanofibres (CNFs) concentrations extracted from pineapple (*Ananas comosus*) leaves on the characteristics of the PVA film. Whereas, pineapple leaves have a purity cellulose amount 62.5% for raw fibre.[17] This result is higher when compared to other natural fibers such as the barks of *Vachellia farnesiana*[33], *Kigelia africana*,[34] and *Cyrtostachys renda*[35] with cellulose content 38.8%, 55.1%, and 45.1%, respectively. The high cellulose content in pineapple leaves make suitable candidate for use in bio-nanocomposite matrices as a reinforcing filler. Thus, this study was aimed to analyze the effect of pineapple leaves extracted CNFs addition on the properties of PVA film, extracted from pineapple leaves, on the properties of PVA film. The bio-nanocomposite film was observed for its surface morphological, tensile strength, functional groups, crystallinity, thermal stability, and transparency. The results of the study are expected to provide a new perspective on the use of CNFs filler incorporated PVA as a bio-packaging material with superior characteristics.

2. Material and methods

2.1. Materials

Polyvinyl alcohol (PVA, 99% hydrolyzed, MW 89,000–98,000 g mol^{-1}) was obtained from Sigma-Aldrich Pte. Ltd, Singapore. Extraction of cellulose nanofibres (CNFs) from pineapple leaves using high-shear homogenisation and ultrasonication was described in previous work.[17] The mean diameter of the CNFs was 68 nm.

2.2. Preparation of PVA film and bio-nanocomposite

PVA film: in a glass beaker, 10 g of PVA granules and 100 mL of distilled water were mixed. The mixture was heated using a magnetic stirrer (Daihan Scientific MSH-200) for 2 h at 70 °C and 500 rpm until gelatinised. An ultrasonic homogeniser sonicated the gel for 5 min at 600 W. The treated gel was cast in a Petri dish and dried in a vacuum drying oven (50 °C, 0.6 MPa, 20 h).

Bio-nanocomposite film: about 10 g PVA granules were dissolved in 100 mL distilled water. The CNFs of concentrations (1, 2, 3, 4, and 5 wt%) was added to the suspension. The suspension was homogenised (WiseTis Homogenizer HG-15D DAIHAN Scientific Co., Ltd Korea) for 5 min (12 000 rpm, room temperature). The mixture was heated by a hot plate magnetic stirrer (Daihan Scientific MSH-200) for 2 h at 75–80 °C until completely gelatinised.[36] The resulting gel was treated using an ultrasonic homogeniser (600 W) for 5 min. After that, the suspension was poured into a glass mould (190 mm × 150 mm) and dried at 50 °C vacuum drying oven for 21 h at 0.6 Mpa.[36] Table 1 displayed the ratios used and the labelling key for each sample. Before sample characterisation, all films were kept in a closed desiccator at 25 °C and 50% relative humidity.

2.3. Characterization techniques

2.3.1. FE-SEM analysis. The PVA film and bio-nanocomposites were placed on the field emission-scanning electron microscope (FE-SEM Quattro S, Thermo Fisher Scientific, Waltham, MA, USA) sample stub. The PVA film and bio-nanocomposite morphological fracture surfaces were observed using FE-SEM at 15 kV. The FE-SEM image of the film was captured at 500 and 2000 magnifications under a high vacuum and working distance of 10 ± 0.5 mm.

2.3.2. XRD analysis. The X-ray diffraction (XRD) testing for PVA film and bio-nanocomposites was carried out using the Shimadzu XRD-700 Maxima X series (Shimadzu Corp., Kyoto, Japan). The sample was scanned at 2θ from 5 to 50° at 40 kV and 30 mA with CuKα radiation ($\lambda = 1.54$). Before XRD testing, samples were oven-dried for 2 h at 60 °C. The crystallinity index (CI) of the sample was calculated using (eqn (1)).[37]

$$CI = [(I_{002} - I_{am})/I_{002}] \times 100 \quad (1)$$

where I_{002} is the intensity of 2θ–22.6°, which corresponds to the crystalline fraction, and I_{am} is the intensity of 2θ–18°, which corresponds to the amorphous fraction.

2.3.3. UV-VIS analysis. The transparency of films was evaluated by Shimadzu UV 1800 spectrophotometer according to ASTM D 1003-00.[23] An equal-weight rectangular sample (10 mm × 25 mm) was placed in the spectrophotometer by a transmittance spectrum of 400 to 800 nm. The transparency film is based on the area under the transmittance curve.

2.3.4. FTIR spectroscopy. The fourier transform infra-red (FTIR) analysis was carried out by using an Attenuated Total Reflectance-Fourier Transform Infra-Red (ATR)-FTIR

Table 1 The composition of bio-nanocomposite films

Samples	PVA (g)	CNFs (wt%)	Distilled water (mL)
PVA film	10	—	100
PVA–CNFs 1%	10	1	100
PVA–CNFs 2%	10	2	100
PVA–CNFs 3%	10	3	100
PVA–CNFs 4%	10	4	100
PVA–CNFs 5%	10	5	100

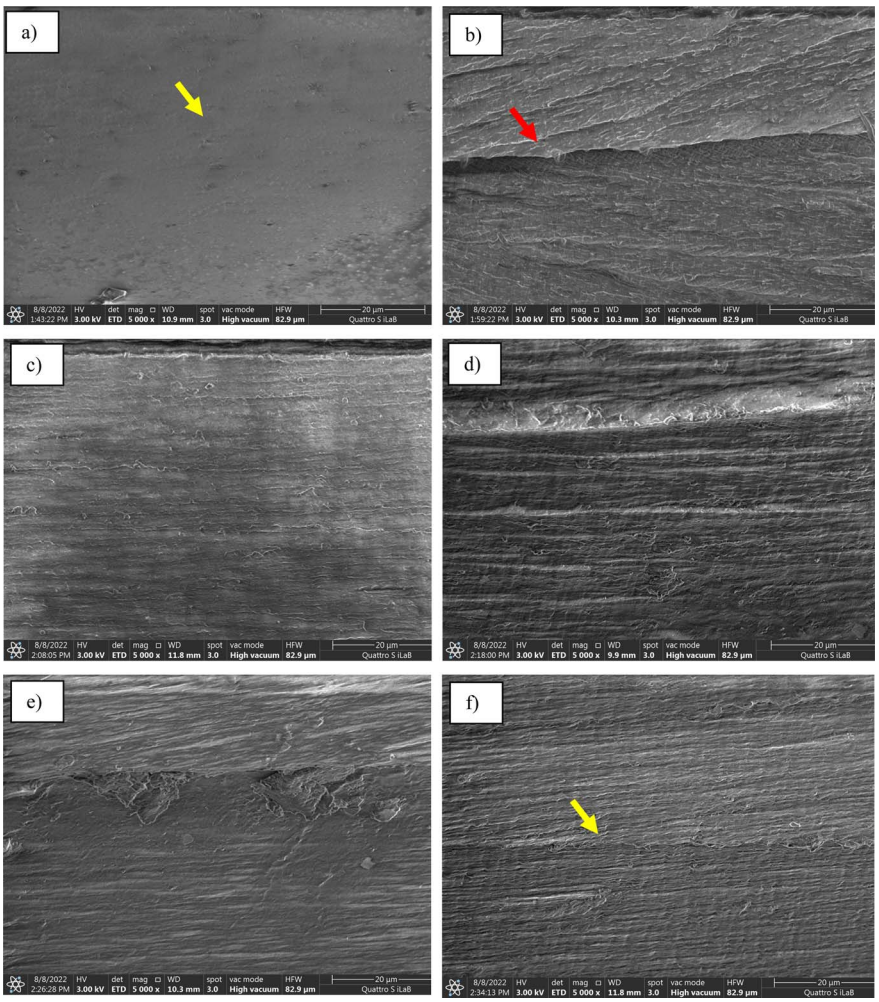

Fig. 1 FE-SEM images of fracture surface for PVA film (a), PVA–CNFs 1% (b), PVA–CNFs 2% (c), PVA–CNFs 3% (d), PVA–CNFs 4% (e) and PVA–CNFs 5% (f).

Table 2 The CI, thermal properties, and transparency of bio-nanocomposite

Samples	CI (%)	T_{max} (°C)	The residue after 550 °C (%)	Transparency (%)
PVA film	74.8	336.3	8.0	86.4
PVA–CNFs 1%	77.7	336.2	7.7	83.6
PVA–CNFs 2%	77.3	334.1	7.4	83.2
PVA–CNFs 3%	77.9	335.6	7.1	86.8
PVA–CNFs 4%	78.8	341.8	5.4	86.0
PVA–CNFs 5%	77.4	341.2	6.2	88.1

spectroscopic equipped with a UATR unit cell from PerkinElmer (Spectrum two) (PerkinElmer Corporation, Waltham, MA, USA). The dried film was scanned between 4000 and 400 cm^{-1} with the sample set on the diamond crystal. The 32 scans per sample were obtained at 4 cm^{-1} resolution. The spectrum at a wavenumber (400–4000 cm^{-1}) was taken by pressing the torque knob with the same pressure.

2.3.5. TGA and DTG analysis. A thermal analysis (thermogravimetry analysis (TGA) and derivative thermogravimetry (DTG)) of samples was monitored on the instrument TGA 4000, PerkinElmer, Hopkinton, MA, USA. About 10 mg of the film was placed on a microbalance inside the furnace. The nitrogen flow rate was set at 20 mL min^{-1}. The test was carried out from 30 to 600 °C. The weight loss and its rate as well as the residue were measured by Pyris software (Version 11, Pyris, Washington, MA, USA).

2.3.6. Mechanical properties. The mechanical properties of PVA film and bio-nanocomposite were investigated following theirs tensile strength and strain at break using the Universal Testing Machine (UTM) (AGS-X series 5 kN, Shimadzu, Japan). The width and thickness of the samples were measured with 0.1 mg accuracy with a precision balance (Kenko). The tensile test speed was 30 mm min^{-1}. The ASTM D638-type V standard was used to prepare the samples. The testing was repeated 5 times for each sample.

2.3.7. Statistical analysis. The significance of the differences in tensile and water absorption properties for loading of different CNFs suspensions in the bio-nanocomposite films was verified using analysis of variance (ANOVA). A significant

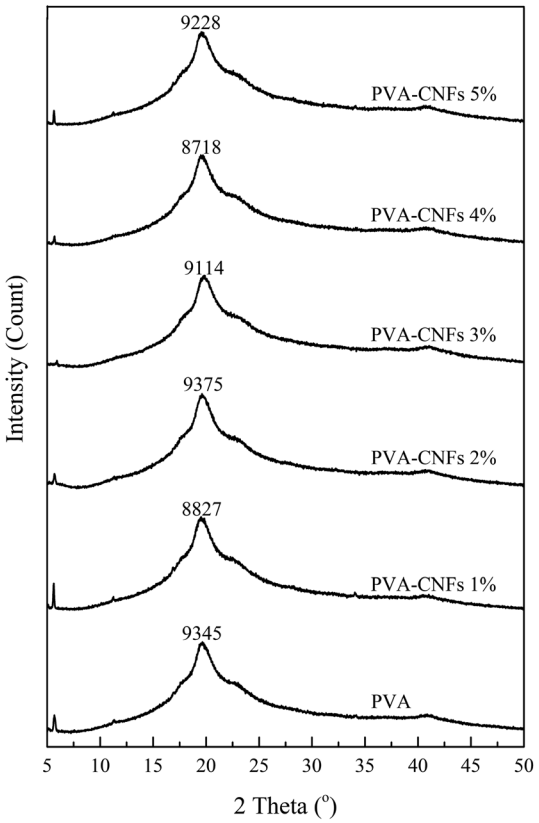

Fig. 2 The XRD patterns of PVA and bio-nanocomposite films.

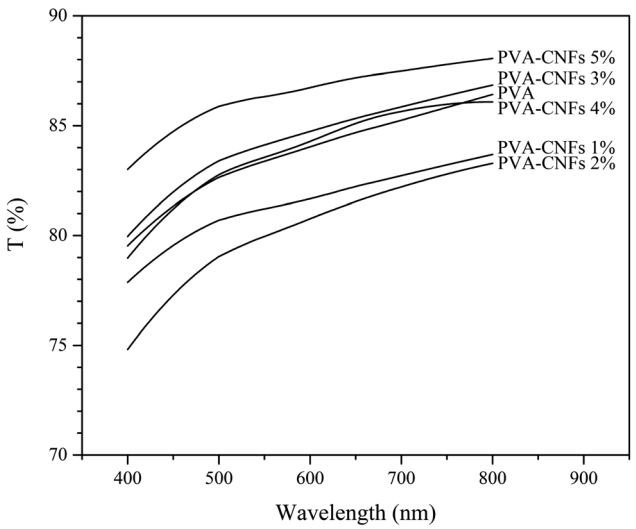

Fig. 3 The UV-VIS of PVA and bio-nanocomposite films.

difference was found at $p \leq 0.05$ and further analysed using Duncan's multiple distance test.

3. Results and discussion

3.1. FE-SEM analysis

The FE-SEM observations provide informations about the presence of voids, the homogeneity of bio-nanocomposites,

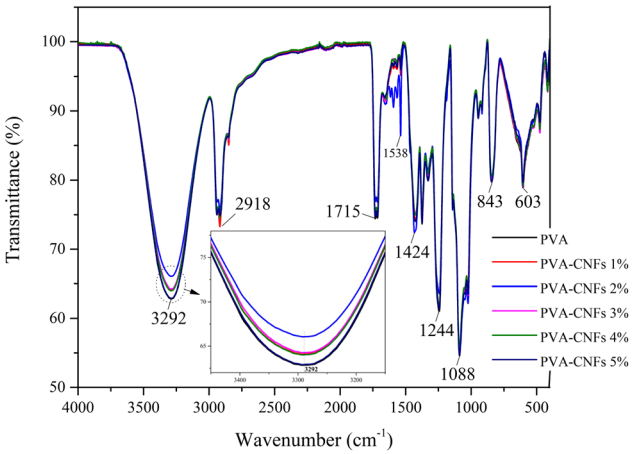

Fig. 4 The FTIR of PVA and bio-nanocomposite films.

agglomerations, distribution, and possible orientation of CNFs in the PVA matrix.[31] FE-SEM photographs of fracture surfaces of PVA film and bio-nanocomposites before and after CNFs incorporation (1–5 wt%) are displayed in Fig. 1. The results showed a change in the microstructure of the films after the addition of CNFs. The delicate surface and a more compact fracture surface were evident in the pure PVA film in Fig. 1a (see yellow arrow) indicates that the homogeneous dispersion of PVA. Fig. 1b–f shows a rougher surface upon the addition of CNFs 1 into PVA matrixes film, suggesting strong adhesive bonding between PVA and CNFs as well as preventing smooth fractures.[20,38] This result was due to the formation of hydrogen bonds between cellulose hydroxyl and PVA hydroxyl groups.[39–41] Observing the individual CNFs dispersions in the PVA matrix was difficult due to the small nanoparticle size. Adding 1 wt% of CNFs changed the microstructure of the fracture surface (Fig. 1b) marked with a red arrow. Homogeneous dispersion caused strong interaction and adhesion between matrix polymer and CNFs surface. The addition of CNFs of different concentrations leads to agglomeration for 1 wt% of CNFs loading with a rougher surface and more clumps in the bio-nanocomposite films with 5 wt% of CNFs (marked with a yellow arrow). In general, no distinctive gaps between the fibre and PVA matrix were visible at the CNFs content up to 4%, indicating good compatibility and dispersion, enabling the fibre to create strong adhesive bonds and thus improving mechanical properties as well as maintaining good transparency, as noted by the following discussion.

3.2. XRD analysis

The crystallinity index (CI) of the bio-nanocomposite film is shown in the Table 2. All films showed peaks at around 5.5 and 20°, which indicated a semi-crystalline structure. Table 2 shows the CI of the bio-nanocomposite film. The addition of CNFs increased the CI for the PVA film was 74.8% while in the case of PVA–CNF 4 wt% it reached 78.8%. The increase in CI increased the tensile strength of bio-nanocomposite (see Fig. 6). The results of CI show that the addition of CNFs led to an increase in

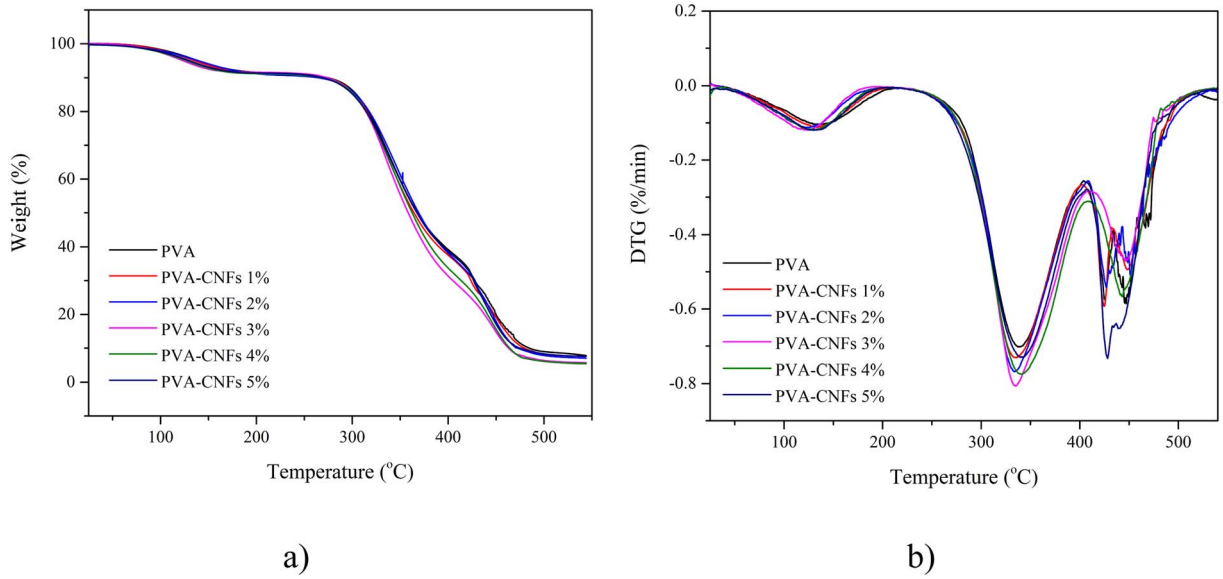

Fig. 5 (a) TGA, and (b) DTG graphs of PVA and bio-nanocomposite films.

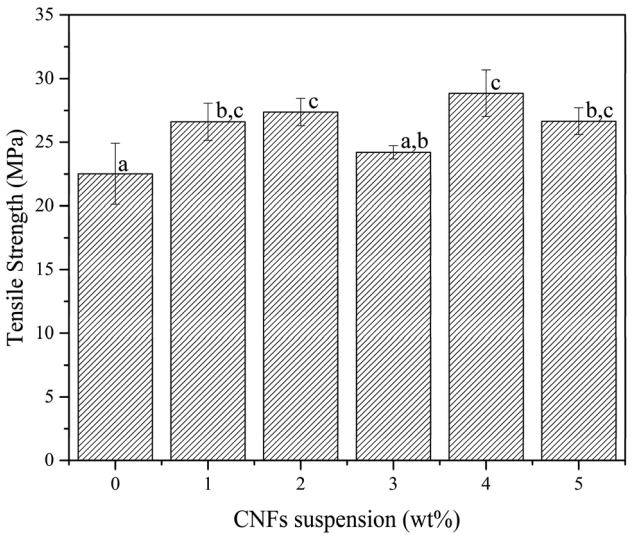

Fig. 6 Tensile strength as a function of CNFs loading.

the crystallinity of the bio-nanocomposites. The high CI phenomenon was also caused by the excellent cellulose nanofibre dispersion in the matrix PVA. The increase in CI was due to the nano dimension of CNFs.[42,43] The nano-sized material has large specific surface area.[29] The high CI of nanocellulose also indicated that the process of downsizing cellulose into nanocellulose through chemical and mechanical processes has succeeded in maintaining the original crystalline structure of cellulose.[44] During the treatment, XRD rays were passed through the sample so that less intensity was captured. This case was similar to that of a previous study.[11] An increase in the CI was explained by a decrease in amorphous phase chain mobility and was supported by previous studies.[45]

3.3. UV-vis analysis

UV-vis barrier properties were one of the key features in developing films for biopackaging. It allows for avoiding or slowing down the oxidation of proteins, lipids, vitamins, or pigments. This characteristic is directly linked to the food shelf life by avoiding unwanted colour, taste, loss of odour, and nutrients, with the presence of organoleptic and nutritional packaged foods.[46,47] Table 2 shows UV-vis light transmittance values and film opacity based on PVA mixtures as control and influence with CNFs (1–5 wt%) in the wavelength range 400–800 nm. The control film had a transmittance of 86.4% and was entirely transparent (Fig. 3). PVA films were known for transparency, and mixtures exhibited transparency due to the high homogeneity of the components. The same transparency was seen in films with up to 5% PVA/CNFs as well, showing excellent CNFs dispersion at nanoscale into the PVA film matrix.[48,49] However, a higher opacity value was detected for 5% PVA/CNFs ($p < 0.05$), principally because of the light travel resistance due to agglomerated CNFs particles as noted by morphology analysis (Fig. 1f). Relatively, all films are considered as highly clear because the UV-vis analysis showed that all films are transparent with a transmission value above 75%. The different transparency of the film is related to the internal structure developed during film drying. This structure, in turn, is strongly influenced by the initial structure of polymer mixing including dispersed and aggregated fractions.[50] The difference in transparency was also influenced by the type of nanocellulose used. The addition of 5 wt% cellulose nanocrystals (CNC) and TEMPO-oxidised cellulose nanofibers (TOCNs) from oil palm empty fruit bunches on poly(methyl vinyl ether maleic acid)/PMVEMA-poly(ethylene glycol)/PEG film showed that the transparency of the film with CNC was higher than TOCNs.[51] Packaging transparency was an essential preference for consumers to see food items in the packaging.

3.4. FTIR spectroscopy

Fig. 4 shows the FTIR analysis of the pure PVA and the bio-nanocomposite. FTIR analysis was aimed to characterize the structural changes due to the incorporation of different amounts of CNFs into the PVA film matrix in the wave number range of 4000–400 cm^{-1} with a spectral resolution of 4 cm^{-1}. This interaction can result in peak shift and peak intensity changes in the bio-nanocomposite films.[9,52] The FTIR spectrum of the pure PVA film revealed a characteristic peak at a broad absorption band between 3000 and 3500 cm^{-1} centred at 3292 cm^{-1}, which corresponded to strain vibration (OH).[53] There are some shift on FTIR curve after addition of CNFs. Strain vibration (OH) shift from 3292 cm^{-1} to 3282 cm^{-1} for PVA–CNFs 2%. This shift is a result of mainly due to the plenty hydroxyl groups between PVA and CNFs, which can form intramolecular and intermolecular hydrogen bonds.[54] The peak doublet at about 2918 cm^{-1} can be assigned to the CH_2 strain vibration. The small band around 1715 cm^{-1} belonged to the (C=O) stretching vibration of the residual poly(vinyl acetate) unit (≤2%) due to the PVA preparation of the hydrolysis of poly(vinyl acetate).[55] The peak at 1424 cm^{-1} belonged to (CH_2) bending vibrations. The (CH_2) vibration caused the peak at 1244 cm^{-1}. The peak at 1088 cm^{-1} was defined (C–C) coupled to the strain vibration (C–O). This peak was related to the crystallinity of PVA.[56] The characteristic peak of 843 cm^{-1} was assigned for a CH_2 vibration.[57]

3.5. TGA and DTG analysis

Fig. 5 shows the TGA and DTG graphs of the PVA films and their bio-nanocomposites at different CNFs contents (1–5 wt%). There were three decomposition steps in the TGA curve. Initially, the sample weight was slightly reduced due to the evaporation of absorbed water (80–110 °C) (Fig. 5a).[58] From 300 to 400 °C, a second sudden weight loss occurred due to the decomposition of the cellulose and PVA matrix.[56] The maximum decomposition rate temperature (T_{max}) of the films during the second weight-loss period is presented in Table 2. After the addition of CNFs to the PVA matrix, the thermal resistance of the films increased. The maximum thermal resistance of PVA/CNFs film 4 wt% is 341.8 °C which is in line with the highest CI of all bio-nanocomposite as shown in Fig. 2. Improved crystal structure resulted in higher heat resistance and increased maximum temperature for thermal decomposition[11] and is in good agreement with a previous study.[18] The thermal stability was affected by the good interfacial bond between the CNFs and PVA matrix; thereby reducing the weight loss in the sample.[59] The T_{max} of PVA was 336.3 °C before the addition of CNFs. In addition, the presence of the extended chain crystals of nanocellulose with hydrogen bonds that were inherently bonded and arranged in an organised manner caused the thermal resistance of PVA composites to be higher.[60] These results corresponded with a previous study by Yihun *et al.* (2021).[49] After further heating, a third weight loss was observed at over 420 °C, resulting from the decomposition of ash.[11] T_{max} increased from 336.3 to 341.8 °C as the addition of CNFs increased by 4 wt%, which confirmed the index crystallisation behaviour of the improved bio-nanocomposite, as shown by the previous XRD results. The increased Tmax indicated a hydrogen interaction between the matrix and CNFs, as the mobility of the polymer chains was limited by the addition of CNFs. It is also confirmed that CNFs promotes matrix crystallisation.

The use of plasticisers on the PVA matrix also determined the thermal properties of the PVA films. It is essential to use plasticisers for PVA in order to control the relevant melting temperature, fluidity, and thermal stability, especially for screw extrusion and injection moulding processes widely used for packaging applications. However, the use of plasticisers must also be controlled. Its exaggerated use is known to result in phase separation due to increased hydrogen bonding between the plasticiser and polymer molecules.[13]

3.6. Mechanical properties

Fig. 6 shows the tensile strength (TS) of pure PVA and bio-nanocomposite film. The pure PVA film had the lowest TS (22.5 MPa) and strain at break (178.4%). PVA–CNFs 4% displayed the highest average TS and SB, with an increment of around 28.0 and 18.5% compared to pure PVA film. This result was attributed to the homogeneity of the CNFs dispersion within the PVA matrix, resulting in good interface hydrogen bonds between the PVA matrix and the cellulose chains anchoring them against movement.[20,45,61] This result is also confirmed by the FE-SEM photographs (Fig. 1), which showed beach marks homogeneously distributed across all the fracture surfaces. It also is related to the increased CI of the bio-nanocomposite film (Table 2), which can improve mechanical properties.[18,38] However, the strength of the bio-nanocomposite film decreased by adding 5 wt% CNFs, attributed to the agglomeration of CNFs in the PVA matrix (Fig. 1f). Furthermore, fibre length is a critical factor in determining film properties, particularly in tensile strength. During gelation, long fibre tended to entangle and increased the surface area of the film. Furthermore, a larger surface area caused the distribution of force applied on the film surface to be wider than short fibre. Longer fibres showed higher tensile strength compared to short fibres.[62]

The SB in PVA and PVA/CNFs 4 wt% increased drastically due to the addition and excellent distribution of CNFs into the PVA matrix and caused the bio-nanocomposite to brittle. It is supported by FE-SEM observation in Fig. 1, showing a strong bonding of matrix and reinforcement, causing the improved tensile strength and CI of PVA–CNFs 1 wt% film. The increase in tensile properties of the bio-nanocomposite films was due to the denser structure. This phenomenon is similar to previous researchers.[11,29]

The tensile strength of thus obtained PVA–CNFs 4 wt% is three times stronger than another biopackaging based on PVA/nanocellulose/Ag nanocomposite films reinforced with 8wt% nanocellulose.[63] Furthermore, our film is also 81% (28.8 MPa) higher than a biocomposite made from polyvinyl alcohol-modified bacterial nanocellulose (5.33 MPa).[64] This result highlighted that the addition of CNFs suspension to the PVA matrix significantly increased the TS ($p \leq 0.05$).

4. Conclusions

The incorporation of CNFs from pineapple leaves enhanced the tensile strength of PVA/CNFs film. The tensile strength of this bio-nanocomposite PVA/CNFs film was considered excellent and flexible to meet the specifications of biopackaging application with some degree of rigidity. The morphological surfaces of the bio-nanocomposite are rougher and clump with increasing CNF concentration in the film. The addition of CNFs also contributed to the improvement of the CI and thermal stability of the PVA film. Therefore, this bio-nanocomposite could be most practical in applications for short-term food storage, for instance, as a novel container for takeaways.

Data availability

Data are available upon request from the authors.

Author contributions

Conceptualization: M. M.; data curation: M. M.; formal analysis: M. M.; funding acquisition: M. A. K.; investigation: M. M., N. M.; methodology: M. M.; project administration: M. M.; resources: E. S., B. H. J., N. H. S.; validation: M. M.; writing – original draft: M. M.; writing – review & editing: M. M., D. A., R. A. I., A. A. S., N. H., M. K.

Conflicts of interest

The authors declare no competing interest.

Acknowledgements

Moonis Ali Khan acknowledges financial support through the Researchers Supporting Project number (RSP2024R345), King Saud University, Riyadh. Saudi Arabia.

References

1 Y. Zoungranan, E. Lynda, K. K. Dobi-Brice, E. Tchirioua, C. Bakary and D. D. Yannick, *J. Environ. Chem. Eng.*, 2020, **8**, 104396.
2 L. Yu, K. Dean and L. Li, *Progress in Polymer Sci.*, 2006, **31**, 576–602.
3 H. Webb, J. Arnott, R. Crawford and E. Ivanova, *Polymers*, 2013, **5**, 1–18.
4 A. Dufresne, *Curr. Opin. Colloid Interface Sci.*, 2014, **19**, 397–408.
5 E. Ojogbo, E. O. Ogunsona and T. H. Mekonnen, *Mater. Today Sustain.*, 2020, **7**, 100028.
6 G. Coppola, M. T. Gaudio, C. G. Lopresto, V. Calabro, S. Curcio and S. Chakraborty, *Earth Syst. Environ.*, 2021, **5**, 231–251.
7 R. Jumaidin, N. A. Diah, R. A. Ilyas, R. H. Alamjuri and F. A. M. Yusof, *Polymers*, 2021, **13**, 1420.
8 S. Mohammadi and A. Babaei, *Int. J. Biol. Macromol.*, 2022, **201**, 528–538.
9 H. Haghighi, M. Gullo, S. La China, F. Pfeifer, H. W. Siesler, F. Licciardello and A. Pulvirenti, *Food Hydrocolloids*, 2021, **113**, 106454.
10 E. Espinosa, I. Bascón-Villegas, A. Rosal, F. Pérez-Rodríguez, G. Chinga-Carrasco and A. Rodríguez, *Int. J. Biol. Macromol.*, 2019, **141**, 197–206.
11 H. Abral, J. Ariksa, M. Mahardika, D. Handayani, I. Aminah, N. Sandrawati, S. M. Sapuan and R. A. Ilyas, *Polym. Test.*, 2020, **81**, 106186.
12 B. Liu, J. Zhang and H. Guo, *Membranes*, 2022, **12**, 347.
13 Z. W. Abdullah, Y. Dong, I. J. Davies and S. Barbhuiya, *Polym. Plast. Technol. Eng.*, 2017, **56**, 1307–1344.
14 N. I. N. Haris, M. Z. Hassan, R. A. Ilyas, M. A. Suhot, S. M. Sapuan, R. Dolah, R. Mohammad and M. R. M. Asyraf, *J. Mater. Res. Technol.*, 2022, **19**, 167–182.
15 M. R. Sanjay, S. Siengchin, J. Parameswaranpillai, M. Jawaid, C. I. Pruncu and A. Khan, *Carbohydr. Polym.*, 2019, **207**, 108–121.
16 A. Vinod, M. R. Sanjay, S. Suchart and P. Jyotishkumar, *J. Clean. Prod.*, 2020, **258**, 120978.
17 M. Mahardika, H. Abral, A. Kasim, S. Arief and M. Asrofi, *Fibers*, 2018, **6**, 28.
18 H. Abral, M. Mahardika, D. Handayani, E. Sugiarti and A. N. Muslimin, *Int. J. Biol. Macromol.*, 2019, **135**, 591–599.
19 H. Abral, M. K. Chairani, M. D. Rizki, M. Mahardika, D. Handayani, E. Sugiarti, A. N. Muslimin, S. M. Sapuan and R. A. Ilyas, *J. Mater. Res. Technol.*, 2021, **11**, 896–904.
20 M. Asrofi, H. Abral, A. Kasim, A. Pratoto, M. Mahardika and F. Hafizulhaq, *J. Eng. Sci. Technol.*, 2018, **13**, 2700–2715.
21 E. Syafri, A. Kasim, H. Abral, Sudirman, G. T. Sulungbudi, M. R. Sanjay and N. H. Sari, *Int. J. Biol. Macromol.*, 2018, **120**, 578–586.
22 M. Asrofi, H. Abral, A. Kasim, A. Pratoto, M. Mahardika, J.-W. Park and H.-J. Kim, *Fibers Polym.*, 2018, **19**, 1618–1625.
23 H. Abral, J. Ariksa, M. Mahardika, D. Handayani, I. Aminah, N. Sandrawati, A. B. Pratama, N. Fajri, S. M. Sapuan and R. A. Ilyas, *Food Hydrocolloids*, 2019, 105266.
24 M. Ramesh, K. Palanikumar and K. H. Reddy, *Renew. Sustain. Energy Rev.*, 2017, **79**, 558–584.
25 Y. G. Thyavihalli Girijappa, S. Mavinkere Rangappa, J. Parameswaranpillai and S. Siengchin, *Front. Mater.*, 2019, **6**, 226.
26 M. R. Sanjay, P. Madhu, M. Jawaid, P. Senthamaraikannan, S. Senthil and S. Pradeep, *J. Clean. Prod.*, 2018, **172**, 566–581.
27 J. Sahari, S. M. Sapuan, E. S. Zainudin and M. A. Maleque, *J. Biobased Mater. Bioenergy*, 2013, **7**, 90–94.
28 F. Hafizulhaq, H. Abral, A. Kasim, S. Arief and J. Affi, *Fibers*, 2018, **6**, 62.
29 M. Mahardika, H. Abral, A. Kasim, S. Arief, F. Hafizulhaq and M. Asrofi, *Lebensm. Wiss. Technol.*, 2019, 108554.
30 N. Noshirvani, W. Hong, B. Ghanbarzadeh, H. Fasihi and R. Montazami, *Int. J. Biol. Macromol.*, 2018, **107**, 2065–2074.
31 K. Choo, Y. C. Ching, C. H. Chuah, S. Julai and N.-S. Liou, *Materials*, 2016, **9**, 644.
32 E. D. M. Teixeira, D. Pasquini, A. A. S. Curvelo, E. Corradini, M. N. Belgacem and A. Dufresne, *Carbohydr. Polym.*, 2009, **78**, 422–431.

33 R. Vijay, J. D. James Dhilip, S. Gowtham, S. Harikrishnan, B. Chandru, M. Amarnath and A. Khan, *J. Nat. Fibers*, 2022, **19**, 1343–1352.
34 M. Ilangovan, V. Guna, B. Prajwal, Q. Jiang and N. Reddy, *Carbohydr. Polym.*, 2020, **236**, 115996.
35 T. M. Loganathan, M. T. H. Sultan, Q. Ahsan, M. Jawaid, J. Naveen, A. U. M. Shah and L. S. Hua, *J. Mater. Res. Technol.*, 2020, **9**, 3537–3546.
36 H. Abral, R. S. Satria, M. Mahardika, F. Hafizulhaq, J. Affi, M. Asrofi, D. Handayani, S. M. Sapuan, I. Stephane and E. Sugiarti, *Starch/Staerke*, 2019, 1800224.
37 L. Segal, J. J. Creely, J. A. E. Martin, C. M. Conrad and L. al. Segal, An Empir. Method Estim. Degree Cryst. Nativ. Cellul. Using X-Ray Diffractom, *J. Text. Res.*, 1959, **29**(10), 786–794.
38 E. Syafri, S. Wahono, A. Irwan, M. Asrofi, N. H. Sari and A. Fudholi, *Int. J. Biol. Macromol.*, 2019, **137**, 119–125.
39 G. G. de Lima, B. D. Ferreira, M. Matos, B. L. Pereira, M. J. D. Nugent, F. A. Hansel and W. L. E. Magalhães, *Carbohydr. Polym.*, 2020, **245**, 116612.
40 J. Ou, S. Hu, L. Yao, Y. Chen, H. Qi and F. Yue, *Chem. Eng. J.*, 2023, **453**, 139770.
41 Y. Xie, Y. Pan and P. Cai, *Ind. Crops Prod.*, 2022, **176**, 114381.
42 H.-J. Kim, S. Roy and J.-W. Rhim, *J. Environ. Chem. Eng.*, 2021, **9**, 106043.
43 Z. Kassab, Y. Abdellaoui, M. H. Salim, R. Bouhfid and M. El Achaby, *Carbohydr. Polym.*, 2020, **245**, 116506.
44 N. Hastuti, K. Kanomata and T. Kitaoka, *J. Polym. Environ.*, 2018, **26**, 3698–3709.
45 A. de Campos, A. R. de Sena Neto, V. B. Rodrigues, B. R. Luchesi, F. K. V Moreira, A. C. Correa, L. H. C. Mattoso and J. M. Marconcini, *Carbohydr. Polym.*, 2017, **175**, 330–336.
46 A. M. Ribeiro, B. N. Estevinho and F. Rocha, *Food Bioprocess Technol.*, 2021, **14**, 209–231.
47 A. T. Petkoska, D. Daniloski, N. M. D'Cunha, N. Naumovski and A. T. Broach, *Food Res. Int.*, 2021, **140**, 109981.
48 X. Niu, Y. Liu, G. Fang, C. Huang, O. J. Rojas and H. Pan, *Biomacromolecules*, 2018, **19**, 4565–4575.
49 F. A. Yihun, S. Ifuku, H. Saimoto and D. A. Yihun, *Cellulose*, 2021, **28**, 2965–2980.
50 R. Villalobos, J. Chanona, P. Hernández, G. Gutiérrez and A. Chiralt, *Food Hydrocolloids*, 2005, **19**, 53–61.
51 N. Hastuti, K. Kanomata and T. Kitaoka, in *IOP Conference Series: Materials Science and Engineering*, IOP Publishing, 2020, vol. 935, p. 12051.
52 R. Shahvalizadeh, R. Ahmadi, I. Davandeh, A. Pezeshki, S. A. S. Moslemi, S. Karimi, M. Rahimi, H. Hamishehkar and M. Mohammadi, *Food Chem.*, 2021, **354**, 129492.
53 T. Riaz, R. Zeeshan, F. Zarif, K. Ilyas, N. Muhammad, S. Z. Safi, A. Rahim, S. A. A. Rizvi and I. U. Rehman, *Appl. Spectrosc. Rev.*, 2018, **53**, 703–746.
54 M. A. Kashfipour, N. Mehra, R. S. Dent and J. Zhu, *Eng. Sci.*, 2019, **8**, 11–18.
55 Y. Hussein, E. M. El-Fakharany, E. A. Kamoun, S. A. Loutfy, R. Amin, T. H. Taha, S. A. Salim and M. Amer, *Int. J. Biol. Macromol.*, 2020, **164**, 667–676.
56 A. Bozdoğan, B. Aksakal, O. Yargi and U. Şahintürk, *Polym. Compos.*, 2020, **41**, 3087–3100.
57 N. F. Farag, S. H. El-Ahmady, E. H. Abdelrahman, A. Naumann, H. Schulz, S. M. Azzam and E.-S. A. El-Kashoury, *Ind. Crops Prod.*, 2018, **124**, 870–877.
58 M. Song, H. Yu, J. Gu, S. Ye and Y. Zhou, *Int. J. Biol. Macromol.*, 2018, **113**, 171–178.
59 L. Han, S. Cui, H.-Y. Yu, M. Song, H. Zhang, N. Grishkewich, C. Huang, D. Kim and K. M. C. Tam, *ACS Appl. Mater. Interfaces*, 2019, **11**, 44642–44651.
60 K. Uetani and T. Kitaoka, *BioResources*, 2021, **16**, 1–4.
61 S. Karimi, A. Dufresne, P. Md. Tahir, A. Karimi and A. Abdulkhani, *J. Mater. Sci.*, 2014, **49**, 4513–4521.
62 H. Fukuzumi, T. Saito and A. Isogai, *Carbohydr. Polym.*, 2013, **93**, 172–177.
63 M. S. Sarwar, M. B. K. Niazi, Z. Jahan, T. Ahmad and A. Hussain, *Carbohydr. Polym.*, 2018, **184**, 453–464.
64 W. Wang, Z. Yu, F. K. Alsammarraie, F. Kong, M. Lin and A. Mustapha, *Food Hydrocolloids*, 2020, **100**, 105411.